FULL PAPER

Predicted results of the velocity structure at the target site of the blind prediction exercise from microtremors and surface wave method as Step-1, Report for the experiments for the 6th international symposium on effects of surface geology on seismic motion

Kosuke Chimoto[1]*, Hiroaki Yamanaka[2], Seiji Tsuno[3] and Shinichi Matsushima[4]

Abstract

1D velocity profiles at a strong motion station in the northern part of the Kumamoto plain, Japan, were submitted in Step-1 of the blind prediction exercise of strong ground motions in the sixth international symposium on effects of surface geology on seismic motion (ESG6). Individual participants were requested to estimate a 1D S-wave velocity profile of sedimentary layers from the given data obtained by microtremor array explorations and surface-wave explorations at the site. This paper reports the target site, methods used by the individual participants, and the submitted results. More than half of the participants estimated the phase velocities of the Rayleigh-wave in the frequency range from 0.53 to 29.8 Hz. The statistical analysis of the phase velocity dispersion curves indicates that the standard deviation was below 40 m/s at the frequencies above 3.4 Hz, and it was below 20 m/s above 20 Hz. The S-wave velocity profiles are also similar to a depth of 20 m. The standard deviation was below 45 m/s. The average S-wave velocity in the top 30 m from the surface is 207.3 ± 60.7 m/s for the submitted profiles. The large variation is related to the introduction of the near-surface low velocity layers. The large variation of the S-wave velocities was found in the deep part. The average S-wave velocity at a depth of 1500 m was 2674 m/s with the standard deviation of 786 m/s. We compared 1D amplifications for the submitted profiles. Common peaks can be identified at 0.3–0.4 Hz and 1–2 Hz, excluding two teams. However, the amplifications vary much in the frequency range higher than 4 Hz. Through the experiment, it was found that the dispersion curves and the shallow S-wave velocity structures are estimated with a low standard deviation among the participants. Further development of the techniques for deep S-wave velocity profiling was found to be required.

Keywords S-wave velocity, Microtremor exploration, Surface-wave exploration, Rayleigh-wave dispersion, Inversion, Kumamoto plain
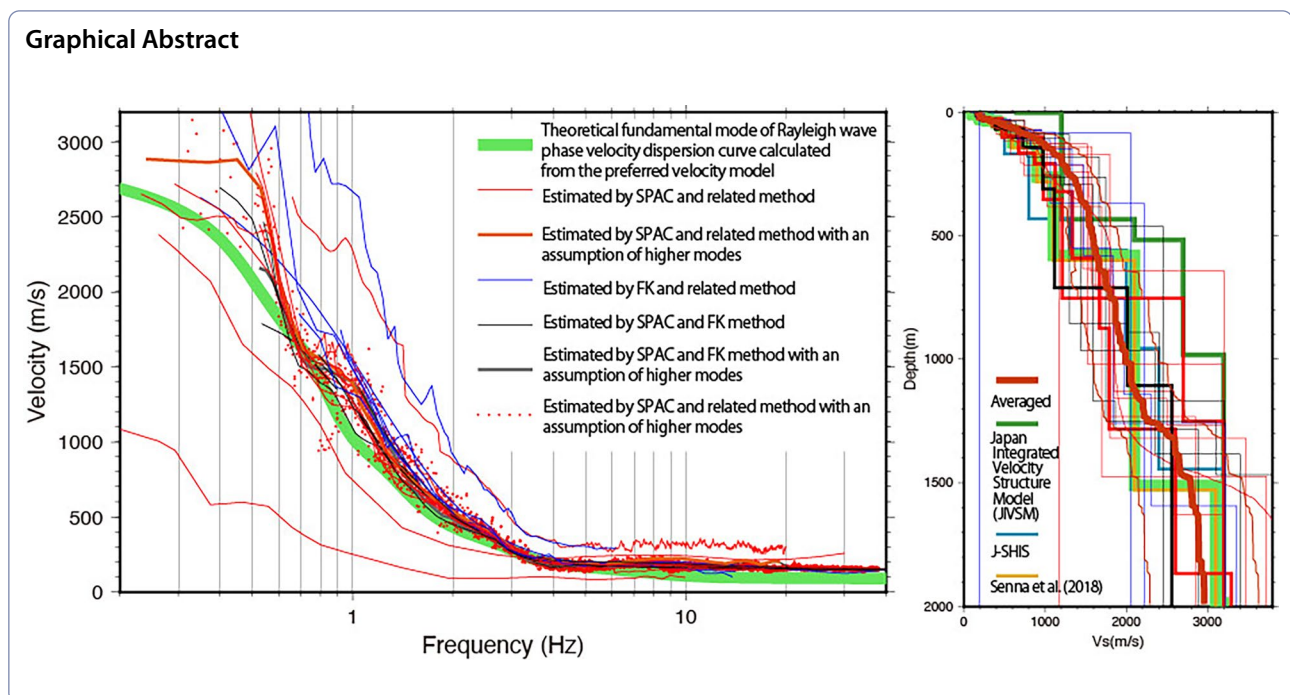
*Correspondence:
Kosuke Chimoto
chimoto.kosuke@kagawa-u.ac.jp
Full list of author information is available at the end of the article

Springer Open

Chimoto *et al. Earth, Planets and Space*   (2023) 75:79

Page 2 of 13

Graphical Abstract

Introduction

The blind prediction exercise of strong ground motions at a site on a sedimentary basin had been conducted in the last international symposia on effects of surface geology on seismic motion (Matsushima et al. 2023 in this special volume). The ground motions were estimated using S-wave velocity (*Vs*) profiles and the observed ground motions at a rock site near the target site. This blind prediction exercise clearly indicates the importance of an accurate *Vs* model beneath and around the target site. Many exploration methods have accordingly been developed to know *Vs* profiles of shallow and deep sedimentary layers. The *Vs* exploration with microtremors (e.g., Okada 2003) have been popular particularly in the ESG (Effects of surface geology on seismic Motion)-related studies because of easy filed operation and well-known surface-wave theory including phase velocity inversions. Therefore, modeling of an *Vs* profile can be included as one of the important steps of the estimation of the ESG.

The blind prediction exercise in the sixth international symposium on effects of surface geology on seismic motion (ESG6) was planned to investigate accuracy and reliability of techniques to predict earthquake ground motions by actual estimations of un-published strong motion records and an *Vs* profile at the target site in Kumamoto Prefecture, Japan (Matsushima et al. 2023). Participants of the blind prediction exercise of the ESG6 were requested to predict an *Vs* profile and earthquake ground motions in three steps. A 1D subsurface *Vs* profile was estimated from microtremor and surface-wave

explorations data at the target site. They were, furthermore, requested to calculate weak and strong ground motions at the target site in the second and third steps (Tsuno et al. 2023 in this special volume). An earthquake record obtained during one of the aftershocks of the 2016 Kumamoto earthquake was selected as the target record in the second step. The strong motion records of the foreshock (14 April) and main shock (16 April) of the 2016 Kumamoto earthquake were then selected for the blind prediction in the third step.

This paper reports the results of the first step (Step-1) of the blind prediction exercise of the ESG6. We compared the *Vs* profiles estimated by the participants. They were also compared with the *Vs* profile derived from a borehole near the target site which was open after the submission of the results of the Step-1 by the participants.

Methods

Passive source and active source measurements were conducted at the target site (Fig. 1). Data acquisition is described in Matsushima et al. (2023). The passive measurements of microtremors were conducted for arrays of five different sizes (KUM-SS1, S, SM, M, LL). Each array consists of two equilateral triangles and seven sensors were used. The combination of the side lengths of the two triangles of each array are (1, 2), (10, 20), (39, 78), (122, 243), and (481, 962) in meters for arrays SS1, S, SM, M, and LL, respectively.

We briefly introduce the methods used by the participants. The participants were requested to submit
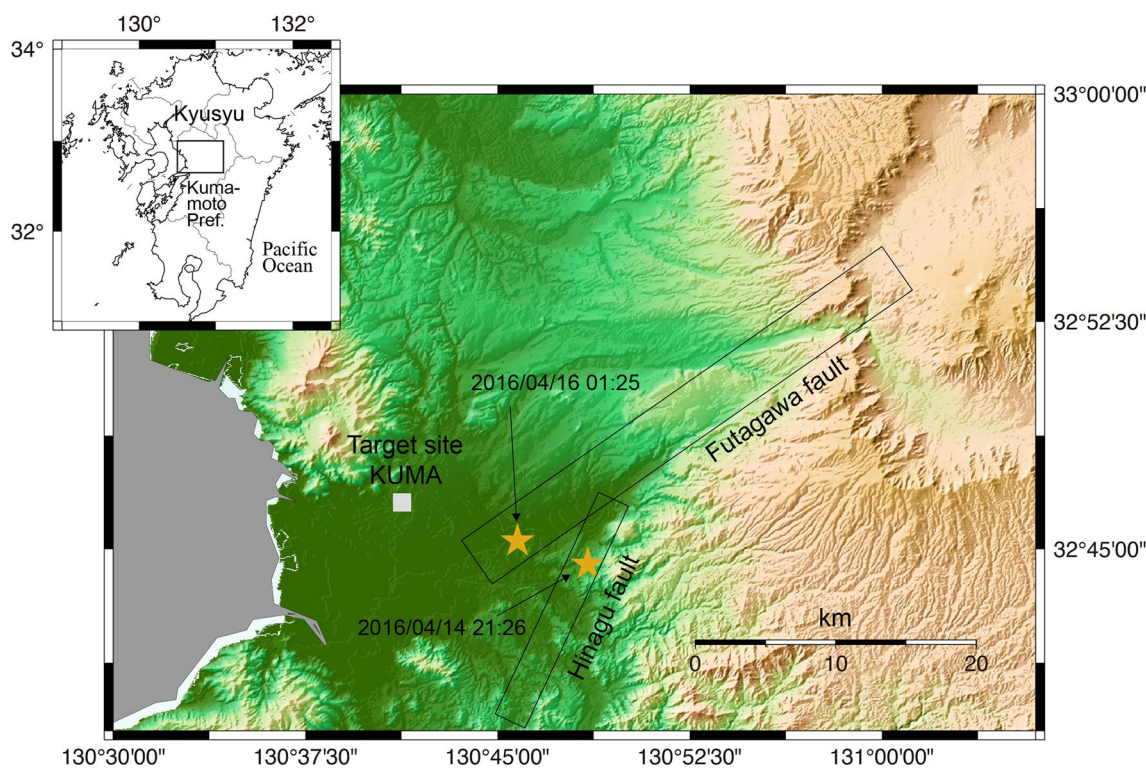
Chimoto *et al. Earth, Planets and Space*   (2023) 75:79

Page 3 of 13

Fig. 1 Map showing the target site KUMA (square). The foreshock and the mainshock of the 2016 Kumamoto earthquakes are shown by stars with the rupture areas associated with the events, shown by rectangular. The inset shows the location of study area

a dispersion curve and a structure model with a simple report. The results for the Step-1 were submitted by 28 teams in total, as shown in Table 1. Fourteen teams participated from Japan, and three teams did from both France and Italy. Two teams participated from Taiwan and Mexico. From Australia, Israel, Iran, Greece and Switzerland one team participated or joined the teams. Several international teams are also included in the participants.

The method used by many teams to estimate phase velocity dispersion curves using the passive data was the SPAC (Spatial Autocorrelation Coefficient) method (Aki 1957; Okada 2003). The multi-mode SPAC method (MMSPAC; Asten and Hayashi 2018), the CCA (Centerless Circular Array) method (e.g., Tada et al. 2007) and the modified SPAC method (Bettig et al. 2001) are included in the SPAC method. The ESAC (Extended Spatial Autocorrelation; e.g., Ohori et al. 2002) was also used by three teams. Eight teams used the FK method to the passive data. The High-Resolution FK (Capon 1969) method is included. The RTBF method (Wathelet et al. 2018) using three components were also used. Several teams used a combination of the methods. The three components high-resolution FK (Poggi and Fäh, 2010) was also applied. The dispersion curves for the respective

arrays using 3C-HRFK and WaveDec (Maranò et al. 2012) were picked in the respective array resolution limits of the arrays. This code estimates the dispersion curves for Love and Rayleigh waves and the ellipticity angle for Rayleigh waves with the maximum likelihood approach.

Not only the vertical components, some teams also analyzed the horizontal components. One team conducted a reorientation of the sensors towards the north direction using a cross-correlation analysis of the horizontal components with respect to a reference station in a frequency range of 0.1 to 0.3 Hz. They have reported misorientations of up to 48°. Two teams used a cross-correlation technique, and one team used only the horizontal-to-vertical spectral ratio instead of the dispersion curve (e.g., Nagashima et al. 2014).

Ten teams used the active source data for the estimation of the dispersion curve. Every team of this group used the FK method in the analysis and the MASW analysis (Park et al. 1999). The effect of the higher modes of the surface waves was also included in the analyses. Many teams used the software of Geopsy (e.g., Wathelet et al. 2020) for the active and passive data, but some teams used the software of BIDO (Tada et al. 2010) in the passive data analysis. The others used in-house softwares. The horizontal-to-vertical spectral ratio (Several abbreviations

Table 1 Participated teams and the method they used

Team	Passive	Active	Inversion
1*	MMSPAC		Direct SPAC
2*	CC	FK + HRLRT	Non-linear neighborhood algorithm
3	MSPAC RTBF 3C(Love) H/V	FK	The Conditional Neighborhood algorithm
4	HRFK RTBF H/V		Neighborhood algorithm
5	SPAC	FK	Iterative inversion
6		MASW	GA
7	ESAC FK MASW		GA with H/V
8	FK	FK	MC
9	MSPAC RTBF CC		Improved neighborhood algorithm
10*	BIDO3.0		An empirical Bayesian approach
11	SPAC		MCMC
12	SPAC		Manual
13	SPAC		Trial and error
14	FK		GA & SA
15	SPAC		GA with H/V
16*	HVR		GA & SA
17	SPAC	FK	GA & SA
18	SPAC ESPAC	FK	GA
19	SPAC CCA		Pelekis and Athanasopulos (2011)
20	ESPAC		GA & SA
21	BIDO		Trial and error
22	FK		simultaneous inversion
23	SPAC	FK	GA
24	FK SPAC	FK	Global/Local/Manual with H/V
25	SPAC		HV-Inv program
26	SPAC	MASW	dinver (Geopsy)
27	FK		MC&SA with MHVSR
28	FK		Herrmann (1991)

The asterisk indicates that their contributions also appeared in the EPS special volume as a published study

are used by teams such as H/V, HVSR, MHVR) was also often used by many participants. The H/V was generally estimated by sensor No. 4 for the M-array or No. 3 for the SM-array. Many teams found two significant peaks in the H/V curve. The predominant peak appears at frequencies between 1.0 to 1.5 Hz. Another peak appears at frequencies between approximately 0.3 and 0.35 Hz. Several participants specified that the predominant frequencies are 1.2, 1.25 and 1.3 Hz. Some teams also identified the deep trough at a frequency of approximately 3.0 Hz. One team conducted a polarization analysis (Burjánek et al. 2010, 2012) and they did not find any signs for two-dimensional polarization effects, whereas another team noted that the 2D effect is observable in the H/V of the large array.

Various techniques were used for the inversion of the dispersion curve. Some teams used primitive techniques of trial-and-error or random search. Some other teams used iterative inversions or non-linear neighborhood algorithm in Geopsy (e.g., Wathelet et al. 2005), a

neighborhood algorithm (e.g., Sambridge 1999; Wathelet et al. 2004) or the Conditional Neighborhood algorithm (Wathelet et al. 2008). Monte Carlo (MC) and modified MC (Socco and Boiero 2008) techniques were also used. Ten teams adopted a heuristic inversions of Genetic Algorithm (GA; Yamanaka and Ishida 1996) or Simulated Annealing (SA). Three teams applied a hybrid method of GA and SA (Yamanaka 2007). The latest techniques such as Bayesian approach (Cho and Iwata 2019) and Markov Chain Monte Carlo (MCMC; e.g., Goodman and Weare 2010; Foreman-Mackey et al. 2013) were also used. One team directly converted the phase velocity in the frequency domain as a velocity structure in the depth domain. One team inverted the *Vs* structure using the method proposed by Herrmann (1991). The participants who also estimated Love-wave dispersion curve used it for a joint inversion.

More than 21 teams reported that they have also estimated H/V curves. Furthermore, the joint inversion of

Chimoto *et al. Earth, Planets and Space*   (2023) 75:79

Page 5 of 13

the dispersion curve with the H/V curve were performed by more than nine teams (e.g., Hobiger et al. 2009; Albarello et al. 2011; García-Jerez et al. 2016; Piña-Flores et al. 2017; García-Jerez and Piña-Flores 2018). Even the H/V curve was not incorporated in the inversion, more than six teams used the H/V curves to check the validity of their estimated profiles. However, the theory behind the forward modeling of the H/V curve varies from team to team. Twelve teams modeled the H/V as an ellipticity of Rayleigh-wave (Nogoshi and Igarashi 1971). Seven teams modeled it with a diffuse field concept or assumption (Sánchez-Sesma et al. 2011; Kawase et al. 2011, 2017). One team assumed the idea of Arai and Tokimatsu (2004, 2005), which takes the effects of the fundamental and higher modes into account.

Several teams specified the relationships between V_P, density and V_S during the inversion. Some used the relationship proposed by Ludwig et al. (1970) and some used Kitsunezaki et al. (1990). Other teams specified that they used results by Brocher (2005), Gardner et al. (1974) and Ohta and Goto (1978). Others used the constant values defined in existing models J-SHIS (NIED 2019) and JIVSM (Koketsu et al. 2009, 2012).

The number of layers assumed in the inversion was generally six to ten. One team assumed eighty layers.

Another team modeled over a thousand layers with a thickness interval of 2.5 m. Some teams set initial models from the existing models, J-SHIS V2 (NIED, 2019) and JIVSM (Koketsu et al. 2009, 2012) for the deep part and KuniJiban (Kuni-jiban 2022) and Chimoto et al. (2016) for the shallow part.

Results

Figure 2 shows the dispersion curves submitted by all the teams. Individual curves are plotted one by one in Additional file 5: Fig. S1 which is reordered from Table 1 to maintain anonymity. Three teams estimated the effective mode of Rayleigh-wave (e.g., Tokimatsu et al. 1992; Asten et al. 2019) shown by bold curve and assumed it for the inversion. The others estimated the fundamental mode of Rayleigh-wave. Two teams estimated higher modes of Rayleigh-wave as well. Two teams submitted fundamental mode of Love wave from the horizontal passive data.

Most of the submitted phase velocities are distributed around the theoretical value calculated for the preferred velocity model which is made by Matsushima et al. (2023). The difference among the methods is not observed clearly. We observe four significant outliers of the estimated dispersion curves in the figure. Two of them are similar to each other, even they used different
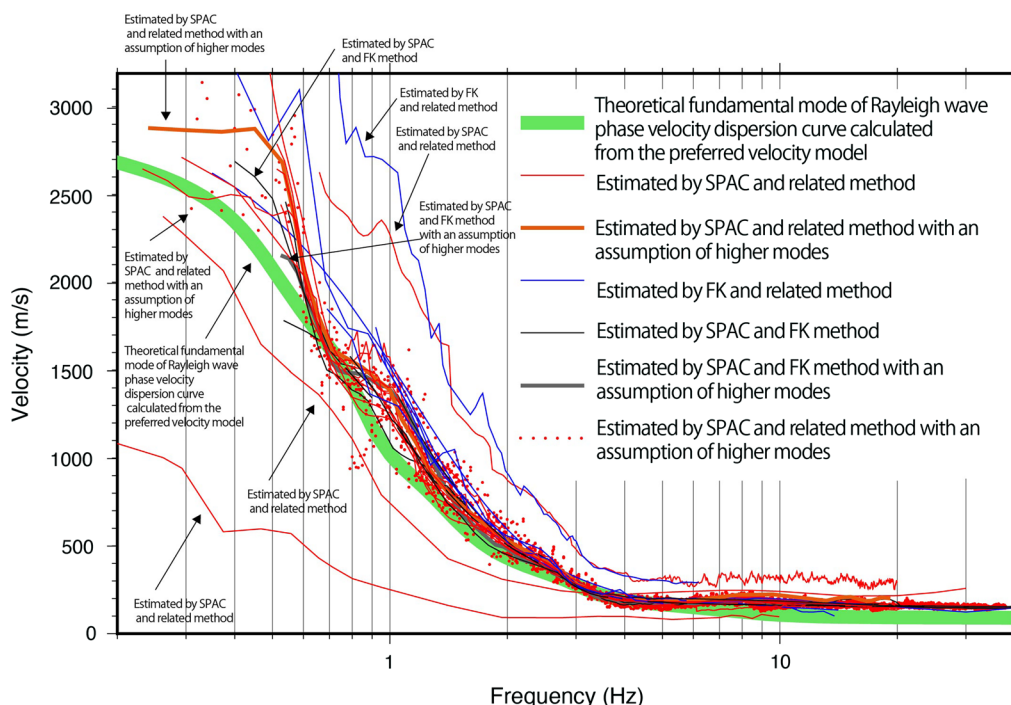

Fig. 2 Rayleigh-wave phase velocity dispersion curve (black). One curve is shown in dots to make easier to see. The curves estimated by the SPAC and related methods are colored by red, whereas the FK and related methods are colored by blue. The curves assumed presence of higher modes of Rayleigh-wave for inversion are shown by bold. Light green curve is the theoretical fundamental mode of Rayleigh-wave phase velocity dispersion curve calculated for the preferred velocity model

Chimoto *et al. Earth, Planets and Space*   (2023) 75:79

Page 6 of 13

methods. Both values are approximately double the values estimated by most teams. We suppose that these two teams made mistakes in the input parameters during the processing of the provided data. One dispersion curve is totally lower than the others. Except for these four curves, all the dispersion curves show similar values and are also similar to the curve calculated theoretically using the preferred velocity model.

We statistically analyzed the submitted dispersion curves. Except for one team who used only the active data, all the teams estimated the dispersion curves in the frequency ranges of 2–5 Hz, as shown in Fig. 3. More than half of the participants estimated the phase velocities in the frequency ranges from 0.53 to 29.8 Hz. Figure 3 also shows the average of the dispersion curves with the standard deviation. The lower the frequency of the phase velocity, the bigger the standard deviation. The average values and the standard deviations of the phase velocities are 2283.4 ± 419.0 m/s at 0.53 Hz, 1322.6 ± 317.0 m/s at 1.00 Hz, 507.6 ± 119.7 m/s at 2.01 Hz, 186.9 ± 35.7 m/s at 5.03 Hz, and 156.1 ± 21.0 m/s at 29.78 Hz. The average curve exhibits higher values than the theoretical one for the preferred velocity model in the frequency ranges of 0.5–0.6 and 0.8–3 Hz. We are still not sure if the reason of this difference is caused by the mixture of the higher modes or not.

Because we found the four outliers in the dispersion curves in Fig. 2, we also analyzed statistically the dispersion curves by excluding these curves. The averaged curve excluding four outliers changed significantly in the

frequency range below 1 Hz. However, it did not show significant change in the high frequency range.

Figure 4 illustrates the frequency ranges, where the phase velocities were estimated by teams. It is ordered in random to maintain anonymity. It is inferred from the figure that all the teams estimated the phase velocities at the lowest frequencies from the LL-array. The minimum and maximum frequencies are significantly depending on the teams. From the analyses of only the passive data, one team estimated the phase velocity at the frequency of approximately 40 Hz. One team estimated the phase velocity at the frequency of approximately 0.2 Hz.

The teams used the active source data estimated the phase velocity at high frequencies above 10 Hz. The maximum frequency of the estimated phase velocity varies from team to team. Even the SS1-array has the smallest size of the array with side-lengths of 1 and 2 m, only five teams used the data of SS1. The SS1 was placed on the same kind of ground with the S-array. Most of the teams estimated the phase velocities at frequencies of 4 to 6 Hz from the data of the S-array, where the velocities are low and constant. One team comments on this point, "We didn't use the SS1-array to calculate phase velocity due to the extremely small radius that may only have a resolution corresponding to a very high-frequency signal using the F–K method". Another team said, "the estimated phase velocity curves obtained from this array tended to be different from it obtained from other arrays, thus it was excluded from the analysis." Another team said, "The miniature array SS1 yields frequencies up to 40 Hz
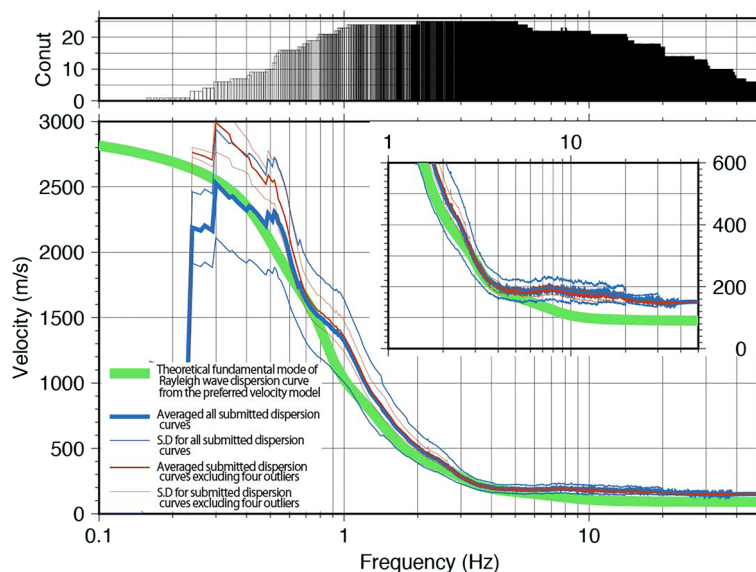

Fig. 3 Average dispersion curve. Blue indicates average dispersion curve and its S.D. for all the models (bottom). Average value and S.D. computed excluding the four outliers is shown by red. Numbers of phase velocities used for average are shown in top against frequency. Light green is calculated for the preferred velocity model. Inset plot shows an enlarged view of the low velocity range
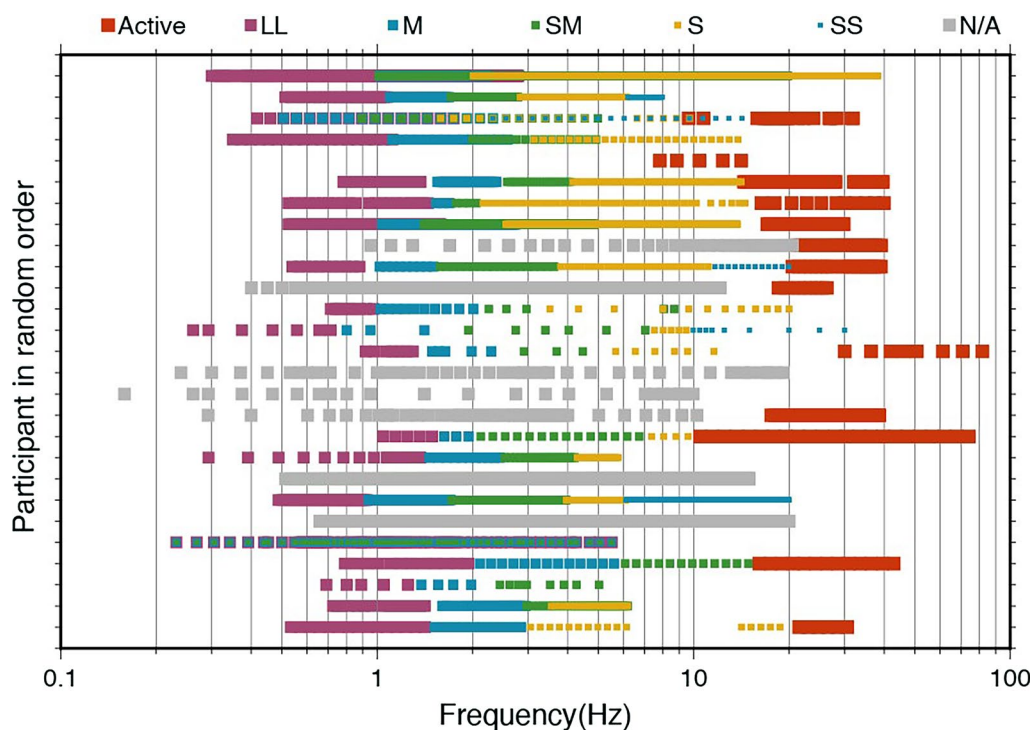
Chimoto *et al. Earth, Planets and Space*   (2023) 75:79

Page 7 of 13

Fig. 4 Frequency bands associated with the dispersive curves is shown by dot. It looks like a continuous line if there are a lot of dots. It is colored by gray if there is no specific report on the range used by the participants

on the MMSPAC curves but the layered earth model produced includes an apparent near-surface compact layer ($Vs_1 = 479$ m/s). However, this layer is not permitted by the MMSPAC curves of array S, hence the array SS1 was discarded."

All the submitted *Vs* profiles are shown in Fig. 5 with the models estimated previously. Individual curves are plotted one by one in the supplementary file (Additional file 6: Fig. S2), which is ordered in the same way, as shown in Additional file 5: Fig. S1. At a depth of 1 m, the average *Vs* among all the participants is 170.8 ± 43.2 m/s, whereas the value of the preferred velocity model is 95 m/s. The preferred model in the shallow part was constructed from the result of the PS-logging. Only a few teams detected the low velocity layers with a *Vs* below 100 m/s. Even though, their depths are shallower than that of the PS-logging. Looking at the individual curves (Fig. 2), several curves show the similar value with that for the preferred model, whereas the averaged phase velocities for all the participants (Fig. 3) are different from the preferred model. One team, who did not use any dispersion curve for the *Vs* modeling, detected the low velocity layer. The average *Vs* is 195.5 ± 46.6 m/s (100 m/s for the PS-logging) at a depth of 5 m, and it becomes 205.1 ± 44.0 m/s at a depth of 10 m (190 m/s for the PS-logging). The *Vs*

values of the preferred velocity model and the averaged model are comparable at the depths of about 10 to 20 m. The average *Vs* is 305.6 ± 102.3 m/s at a depth of 30 m (260 m/s for the PS-logging). The standard deviation (S.D.) of the *Vs* until a depth of 30 m from the surface is not large, whereas the S.D. becomes large below 30 m. Similar trend can be seen at depths from 30 to 50 m in both the preferred model and the averaged model. The *Vs* values of the preferred model are within the variation of the S.D. at these depths. It should be noted that the PS-logging data are not available below 40 m depth, to construct the preferred velocity model.

The deep part below 50 m has much larger variation of the *Vs*. Until a depth to 600 m, *Vs* of the preferred model are generally lower than the average values. The *Vs* values of the basement are different among the teams. However, most of the teams estimated shallower depth to the layer with a *Vs* of above 3 km/s. The basement depth is about 1.5 km in the preferred model, whereas many teams estimated the depth of approximately 1.3 km. The difference due to the methods is also not observable.

We quantitatively compared the models by individual participant with the preferred velocity model. The average of absolute percentage errors (APE) of the *Vs* at the *ith* depth of the submitted *jth* model Vs_i^j and the preferred model Vs_i^P was defined as

Chimoto *et al. Earth, Planets and Space* (2023) 75:79
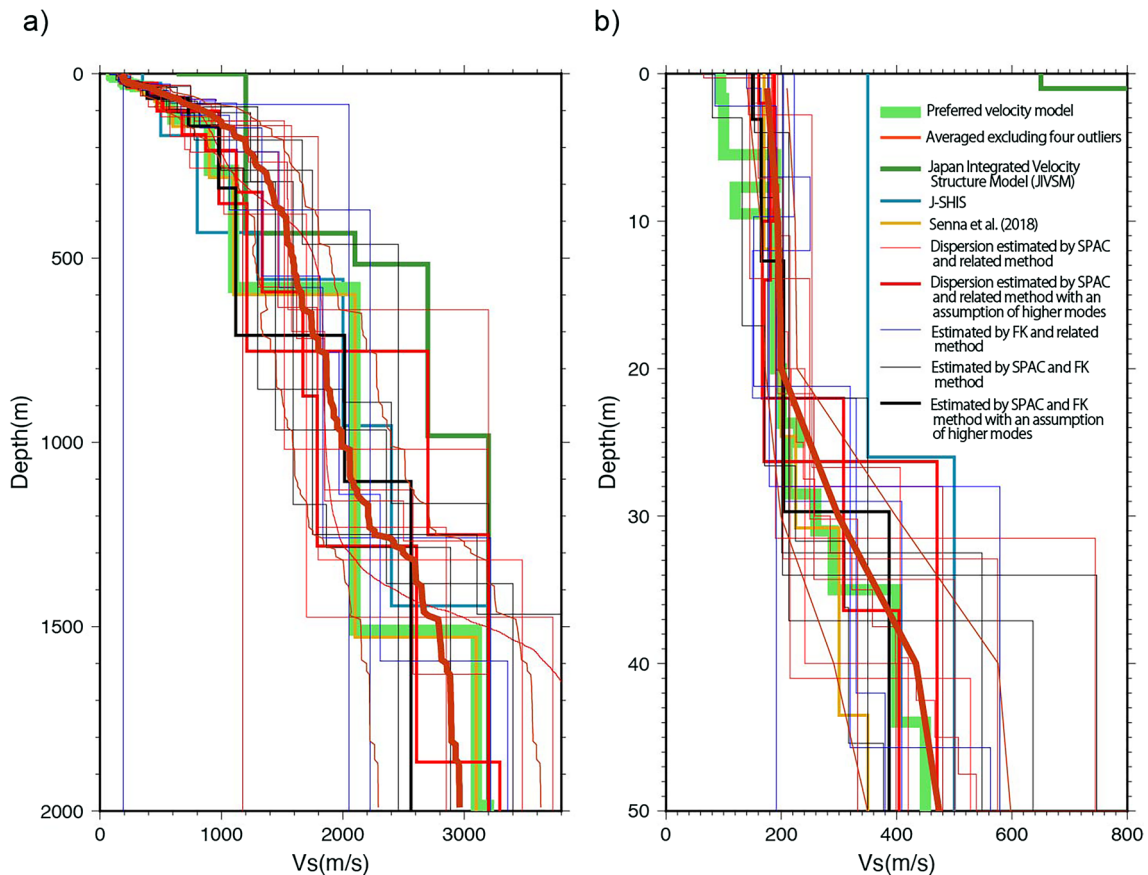
Page 8 of 13

Fig. 5 *Vs* profiles estimated by participants using the SPAC and related methods (red) and profiles using the FK and related methods (blue) and the both (black), except for the models estimated from the four outliers. The profile assumed presence of higher modes of Rayleigh-wave is shown by bold curve. The average and S.D were computed by excluding four outliers and only used active source (red). Yellow-green, blue, green and yellow indicate the profiles for preferred, J-SHIS (NIED 2019), JIVSM (Koketsu et al. 2009, 2012) and Senna et al. (2018) models. **b** Shows the enlarged view of shallow part (**a**)

$$\text{APE} = \frac{1}{M} \sum_{i=1}^{M} \frac{\left| Vs_i^j - Vs_i^P \right|}{Vs_i^P} \qquad (1)$$

where M is a number of the *Vs* to be compared. Left of Fig. 6 shows the APEs for the *Vs* to the depth of the bottom layer of each model. The APEs for most of the submitted models are from 20 to 40% with an average value of 30%, except for the outlier models. The right panel of the figure also shows the APEs for a depth to the top of the layer with the *Vs* more than 400 m/s. The APEs for the shallow parts have the similar distributions as those of the deep layers in the left panel.

It is interesting to focus on the time-average *Vs* to the depth to 30 m (*Vs30*) considering a relation with the ground motion amplification. The *Vs30* is 194.6 ± 36.1 m/s in the average model, whereas the value from the PS logging is 162.8 m/s. Even excluding

four outliers found in the dispersion curves and the model by a team who used only the active source data, the average *Vs30* of the submitted models becomes 185.1 ± 22.4 m/s. The difference seems a bit large. This difference may have been caused by the difference in the upper several meters, where most of the teams did not detect the very low velocity layers as mentioned above. The time-average *Vs* to the depth of 5 m is 171.5 ± 28.8 m/s and it is 180.0 ± 25.8 m/s to 10 m depth (Fig. 7). Compared with that for the preferred model, the time-average *Vs* to the depth of 5 m is more than 1.7 times larger than that of the preferred model. This difference could be possibly, because the result of the PS-logging is in error due to an instrumental issue, or due to the change in near-surface ground condition.

Time-average *Vs* (Garofalo et al. 2016) is also computed. The time-average *Vs* in the topmost *z* meters is defined as
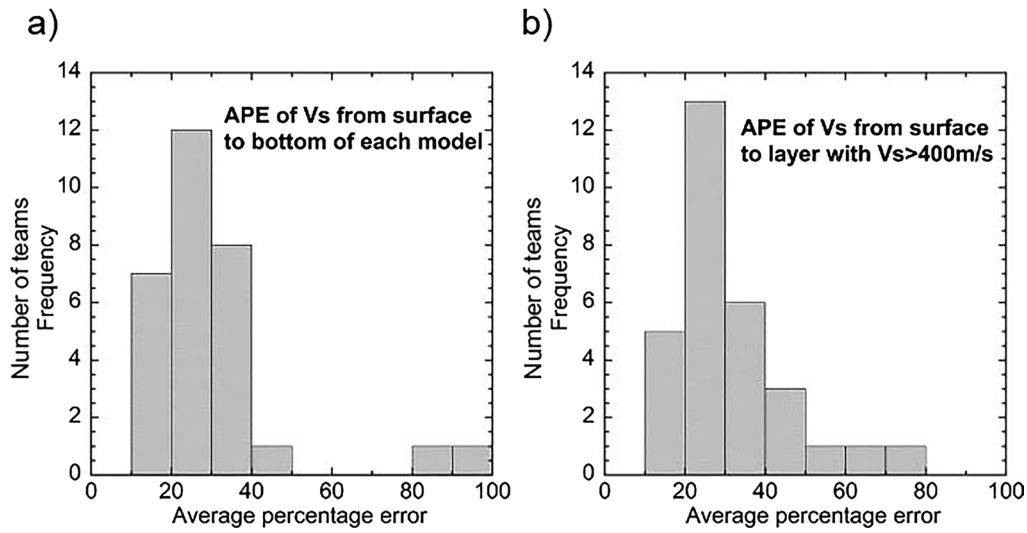
Fig. 6 Distribution of averages of absolute percentages errors (APEs) of *Vs* of individual models with those of preferred one. APEs of *Vs* to the bottom layer of each model (**a**) and to the layer having *Vs* more than 400 m/s (**b**)
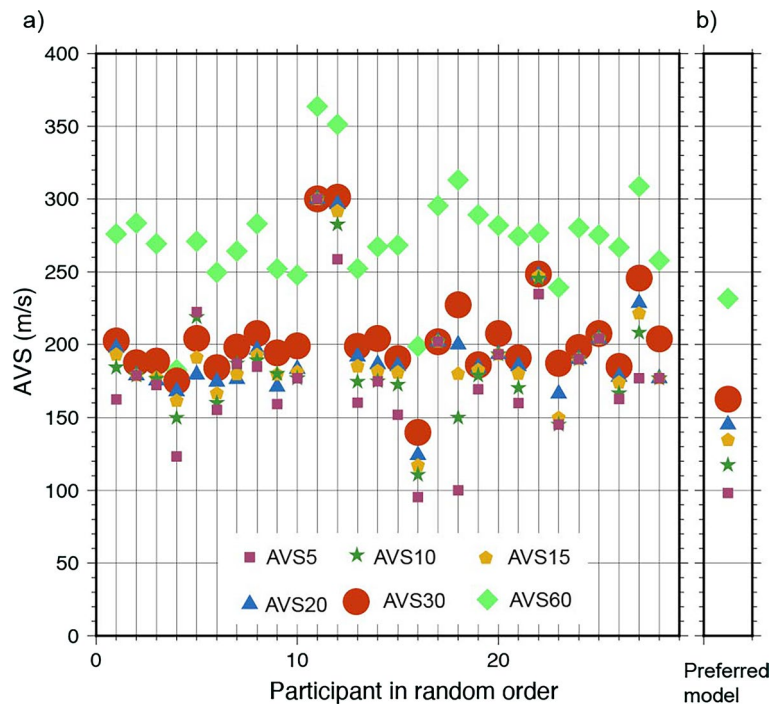

Fig. 7 Average *Vs* to depths of 5, 10, 15, 20, 30 and 60 m from the surface for the submitted profiles (**a**) and for the preferred model (**b**)

$$V_{S,z} = \frac{z}{\sum_{i=1}^{N} H_i/V_{S,i}} \qquad (2)$$

in which N is the number of layers used for the discretization of the model from the surface to z, and H_i and $V_{S,i}$ are the thickness and *Vs* for each layer i, respectively. The value for z of 30 m is referred to as the *Vs30*, for example.

Figure 8 shows the time-average *Vs*. It seems that the variation of the $V_{s,z}$ becomes gentle. However, $V_{s,z}$ of the preferred velocity model is generally lower than those of the submitted models. The distribution of $Vs_{,100} - Vs_{,200}$ seems to follow a normal distribution. However, the Vs,z below 1250 m seems to be clustered in three groups. Two teams show the *Vs* of approximately 1.9 km/s at a depth
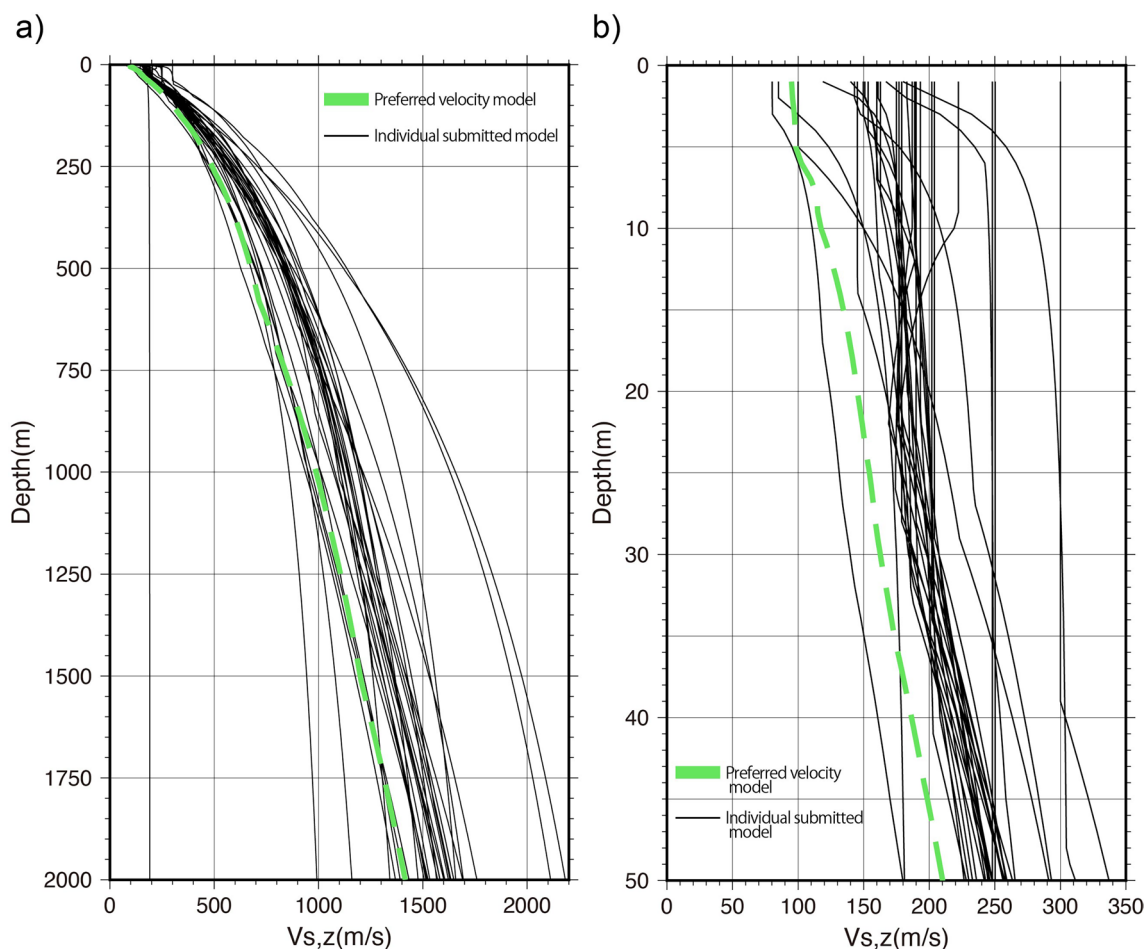
Chimoto *et al. Earth, Planets and Space*   (2023) 75:79

Page 10 of 13

Fig. 8 Time-average *Vs*. Light green and black curves indicate *Vs,z* for the preferred and the submitted models. **a**, **b** Show the deep and shallow parts, respectively

of 1.5 km. They are the teams who estimated significantly higher phase velocity than others (see Fig. 2). Some teams show approximately 1 km/s at a depth of 1.5 km, and many other teams show approximately 1.3 km/s. These teams did not estimate the high *Vs* layers, which corresponds to the seismic bedrock.

In the shallow part, the $V_{s,z}$ of the models are significantly faster than that of the preferred model. This result could be inferred from the differences found in the dispersion curves as seen above.

Discussion

The site effects would be significantly important in the prediction of the ground motion at the target site. We, therefore, discuss about the 1D S-wave amplification characteristic computed for the submitted structure models. Figure 9 shows the computed 1D amplification using the Haskell's matrix method. Infinite Q values are assumed for all the layers in the calculation. It is noted

that we used all the layers in the submitted models in the calculation. This means that the S-wave velocities of the bottom layers are different among the models. The amplification computed for the preferred velocity structure model is also shown in the figure. Except for one curve, all the amplifications show large amplification values at frequencies between 1 and 2 Hz. Many curves show peaks at the frequency range from 0.3 to 0.4 Hz. In the high frequency range above 4 Hz, the amplification values fluctuate around the amplification value of about ten. However, these trends are similar among all the curves. The averaged amplification characteristic among all the amplifications exhibits similar trends with that for the preferred model. However, the amplification for the preferred velocity model exhibits a bit larger value than the averaged one in the entire frequency band. Furthermore, we calculated the APEs for the amplifications for the individual model with that of the preferred velocity model, as shown in Fig. 10. Most of the models have
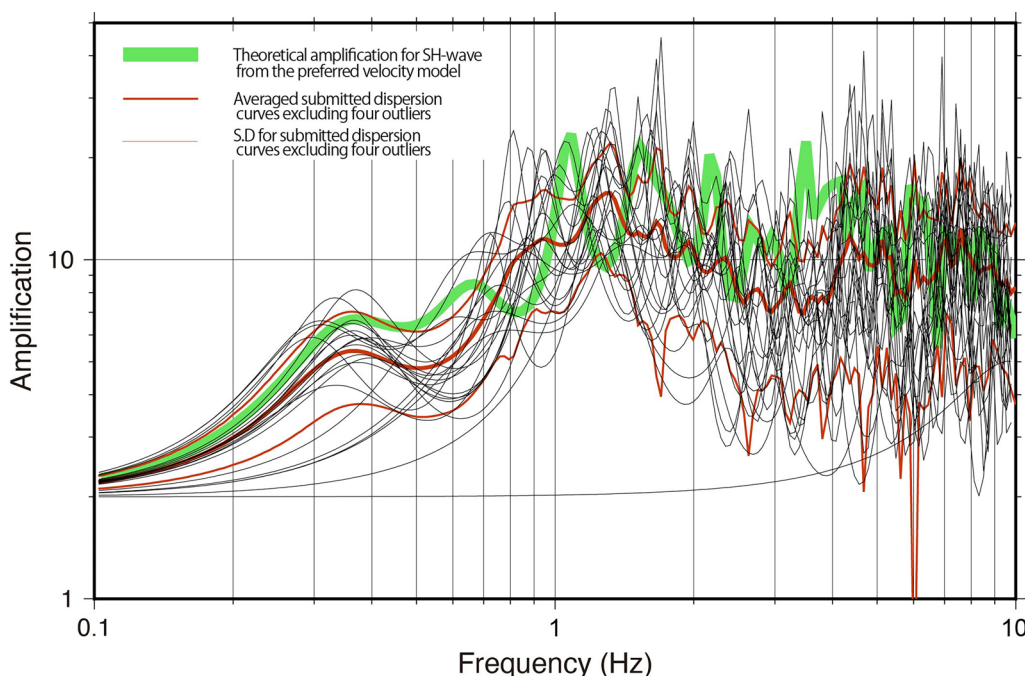
Chimoto *et al. Earth, Planets and Space*   (2023) 75:79

Page 11 of 13

Fig. 9 S-wave amplification characteristic for the vertical incident wave. Green indicates that computed for the preferred velocity model. Red is the averaged value among the amplification characteristics and its S.D. excluding those computed for four outliers
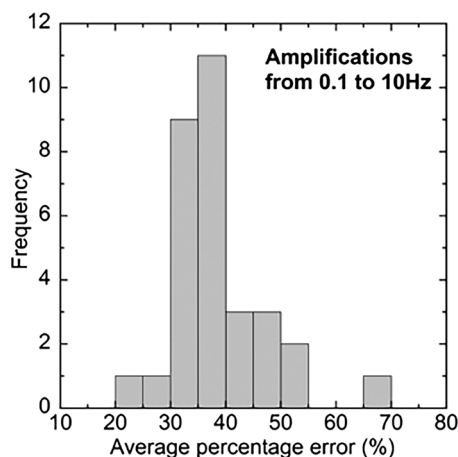

Fig. 10 Distribution of averages of absolute percentages errors of amplifications at frequencies from 0.1 to 10 Hz for individual models with those of preferred one

errors of 30–40%, which is slightly larger than those of the S-wave velocity structure models in Fig. 6.

Conclusions

This paper explains the methods used by the individual participants, and the results in the Step-1 of the blind prediction exercise in ESG6. The phase velocity dispersion curve of Rayleigh-wave in the frequency range from 0.8 to 15 Hz was estimated by most of the participants. The comparison of the dispersion curves indicates that they are very similar in the frequency range from 3 to 40 Hz. Most of the submitted dispersion curves in the frequency range from 0.6 to 40 Hz are similar to the theoretical one for the velocity model derived from the velocity logging. The estimated phase velocities at frequencies lower than 0.8 Hz are larger than the theoretical one. The submitted *Vs* profiles are also similar to the depth of 50 m. It is, therefore, concluded that the *Vs30* can be reliably estimated from active and passive surface-wave data. However, the estimated dispersion curves are larger than that of the logging profile. The large variation of the *Vs* is identified in the deep part because of the large variation of the phase velocities at low frequencies. These results clearly indicate high accuracy of the existing techniques for the shallow S-wave velocity profiling and further need to develop techniques for more reliable deep *Vs* profiling (Additional files 1, 2, 3, 4).

Abbreviations

ESG	Effects of Surface Geology on Seismic Motion
SPAC	Spatial Autocorrelation Coefficient
CCA	Centerless Circular Array
ESAC	Extended Spatial Autocorrelation

Chimoto *et al. Earth, Planets and Space*   (2023) 75:79

Page 12 of 13

Supplementary Information

The online version contains supplementary material available at https://doi.org/10.1186/s40623-023-01842-3.

Additional file 1. Data of the dispersion curve that are averaged for all the results submitted by the participants and their standard deviation.

Additional file 2. Data of the dispersion curve that are averaged for all the results submitted by the participants excluding four outliers and their standard deviation.

Additional file 3. Data of the S-wave velocity structure that are averaged for all the results submitted by the participants and their standard deviation.

Additional file 4. Data of the S-wave velocity structure that are averaged for all the results submitted by the participants excluding four outliers and their standard deviation.

Additional file 5: Fig. S1. Each dispersion curveshowing on all the submitted curves. Grey is the preferred model for Rayleigh-wave fundamental mode.

Additional file 6: Fig. S2. Each S-wave velocity structure modelshowing on all the submitted models. Gray indicates the preferred model.

Acknowledgements

Author contributions
The structure of the manuscript was decided by YH, ST, SM and KC. All authors reviewed the manuscript draft and revised it. All authors read and approved the final manuscript.

Funding

Availability of data and materials
We provide the digital data of the dispersion curve and the S-wave velocity structure that are averaged for the data submitted by the participants as supplementary files. The digital data of the curves that were submitted by participants are not available.

Declarations

Competing interests
Not applicable.

Author details
[1]Kagawa University, 2217-20 Hayashi-Cho, Takamatsu, Kagawa 761-0396, Japan. [2]Tokyo Institute of Technology, 4259 Nagatsuta-Cho, Midori-Ku, Yokohama, Kanagawa 227-8503, Japan. [3]Railway Technical Research Institute, 2-8-38 Hikari-Cho, Kokubunji-Shi, Tokyo 185-5840, Japan. [4]Disaster Prevention Research Institute, Kyoto University, Gokasho, Uji, Kyoto 611-0011, Japan.

References

Aki K (1957) Space and time spectra of stationary stochastic waves, with special reference to microtremors. Bull Earthq Res Inst 35:415–456

Albarello D, Cesi C, Eulilli V, Guerrini F, Lunedei E, Paolucci E, Pileggi D, Puzzilli LM (2011) The contribution of the ambient vibration prospecting in seismic microzoning: an example from the area damaged by the April 6 2009 L'Aquila (Italy) earthquake. Bollettino Di Geofisica Teorica Ed Applicata 52:513–538

Arai H, Tokimatsu K (2004) S-Wave velocity profiling by inversion of microtremor H/V spectrum. Bull Seism Soc Am 94(1):53–63

Arai H, Tokimatsu K (2005) S-Wave velocity profiling by joint inversion of microtremor dispersion curve and Horizontal-to-Vertical (H/V) spectrum. Bull Seism Soc Am 95(5):1766–1778

Asten MW, Stephenson WJ, Hartzell S (2019) Spatially averaged coherencies (krSPAC) and Rayleigh effective-mode modeling of microtremor data from asymmetric arrays. Geophysics 84(3):EN47–EN56

Asten MW, Hayashi K (2018) Application of the spatial auto-correlation method for Shear-Wave velocity studies using ambient noise. Surv Geophys 39(4):633–659

Bettig B, Bard PY, Scherbaum FS, Riepl J, Cotton F, Cornou C, Hatzfeld D (2001) Analysis of dense array noise measurements using the modified spatial auto-correlation method (SPAC): application to the Grenoble area. Bollettino Di Geofisica Teorica Ed Applicata 42(3–4):281–304

Brocher TM (2005) Empirical relations between elastic wave speeds and density in the Earth's crust. Bull Seism Soc Am 95(6):2081–2092

Burjánek J, Gassner-Stamm G, Poggi V, Moore JR, Fäh D (2010) Ambient vibration analysis of an unstable mountain slope. Geophys J Int 180(2):820–828

Burjánek J, Moore JR, Freddy X, Molina Y, Fäh D (2012) Instrumental evidence of normal mode rock slope vibration. Geophys J Int 188(2):559–569

Capon J (1969) High-resolution frequency-wavenumber spectrum analysis. Proc the IEEE 57(8):1408–1418

Chimoto K, Yamanaka H, Tsuno S, Miyake H, Yamada N (2016) Estimation of shallow S-wave velocity structure using microtremor array exploration at temporary strong motion observation stations for aftershocks of the 2016 Kumamoto earthquake. Earth Planets Space 68:206. https://doi.org/10.1186/s40623-016-0581-3

Cho I, Iwata T (2019) A Bayesian approach to microtremor array methods for estimating shallow S wave velocity structures: identifying structural singularities. J Geophys Res 124(1):527–553

Foreman-Mackey D, Hogg DW, Lang D, Goodman J (2013) emcee: the MCMC Hammer. Publ Astronom Soc Pac 125(925):306–312

García-Jerez A, Piña-Flores J, Sánchez-Sesma FJ, Luzón F, Perton M (2016) A computer code for forward calculation and inversion of the H/V spectral ratio under the diffuse field assumption. Comput Geosci 97:67–78

García-Jerez A, Piña-Flores J (2018) A software for inversion of H/V spectral ratios of ambient noise based on the Diffuse Field Approximation. https://w3.ual.es/GruposInv/hv-inv/. Accessed 25 Sep 2022

Gardner GHF, Gardner LW, Gregory AR (1974) Formation velocity and density—the diagnostic basics for stratigraphic traps. Geophysics 39(6):770–780

Garofalo F, Foti S, Hollender F, Bard PY, Cornou C, Cox BR, Ohrnberger M, Sicilia D, Asten M, Di Giulio G, Forbriger T, Guillier B, Hayashi K, Martin

Chimoto *et al. Earth, Planets and Space*   (2023) 75:79

Page 13 of 13

A, Matsushima S, Mercerat D, Poggi V, Yamanaka H (2016) InterPACIFIC project: comparison of invasive and non-invasive methods for seismic site characterization. Part I: intra-comparison of surface wave methods. Soil Dyn Earthq Eng 82:222–240

Geopsy (2022), http://www.geopsy.org/. Accessed 25 Sep 2022

Goodman A, Weare J (2010) Ensemble samplers with affine invariance. Commun Appl Math Comput Sci 5(1):65–80

Herrmann RB (1991) Surface wave inversion program (from computer program in Seismology volume IV)

Hobiger M, Bard PY, Cornou C, Le Bihan N (2009) Single station determination of Rayleigh wave ellipticity by using the random decrement technique (RayDec). Geophys Res Lett 36(14):L14303

Kawase H, Sanchez-Sesma FJ, Matsushima S (2011) The optimal use of horizontal-to-vertical spectral ratios of earthquake motions for velocity inversions based on diffuse-field theory for plane waves. Bull Seism Soc Am 101(5):2001–2014

Kawase H, Mori Y, Nagashima F (2017) Difference of horizontal-to-vertical spectral ratios of observed earthquakes and microtremors and its application to S-wave velocity inversion based on the diffuse field concept. Earth, Planets and Space 70:1. https://doi.org/10.1186/s40623-017-0766-4

Kitsunezaki C, Goto N, Kobayashi Y, Ikawa T, Horike M, Saito T, Kurota T, Yamane K, Okuzumi K (1990) Estimation of P- and S- wave velocity in deep soil deposits for evaluating ground vibrations in earthquake. J Japan Soc Nat Disaster Sci 9:1–17 (**in Japanese**)

Koketsu K, Miyake H, Afnimar TY (2009) A proposal for a standard procedure of modeling 3-D velocity structures and its application to the Tokyo metropolitan area. Japan Tectonophysics 472(1–4):290–300

Koketsu K, Miyake H, Suzuki H (2012) Japan Integrated Velocity Structure Model Version 1, Proceedings of the 15th World Conference on Earthquake Engineering, Lisbon, Portugal, Oct. 12–17, Paper No. 1773.

Kuni-jiban (2022) Web search system for National land subsoil information, https://www.kunijiban.pwri.go.jp. Accessed 23 Sep 2022

Ludwig WJ, Nafe JE Drake CL (1970) Seismic Refraction, the Sea. Vol. 4 (Part 1), Wiley-Interscience, New York, 53–84.

Maranò S, Reller C, Loeliger HA, Fäh D (2012) Seismic waves estimation and wavefield decomposition: application to ambient vibrations. Geophys J Int 191(1):175–188

Matsushima S, Yamanaka H, Tsuno S, Chimoto K, Suzuki H, Kawase H (2023) Investigation of the subsurface structure at the target site in Kumamoto, Japan and the distributed data of the blind prediction exercise, Report for the experiments for "The 6th International Symposium on Effects of Surface Geology on Seismic Motion", submitted to this special volume.

Nagashima F, Matsushima S, Kawase H, Sánchez-Sesma FJ, Hayakawa T, Satoh T, Oshima M (2014) Application of horizontal-to-vertical (H/V) spectral ratios of earthquake ground motions to identify subsurface structures at and around the K-NET site in Tohoku, Japan. Bull Seism Soc Am 104(5):2288–2302

National Research Institute for Earth Science and Disaster Resilience (2019) J-SHIS, National Research Institute for Earth Science and Disaster Resilience https://doi.org/10.17598/nied.0012

Nogoshi M, Igarashi T (1971) On the amplitude characteristics of microtremor (part 2) (in Japanese with English abstract). J Seism Soc Japan 24:26–40

Ohori M, Nobata A, Wakamatsu K (2002) A comparison of ESAC and FK methods of estimating phase velocity using arbitrarily shaped microtremor arrays. Bull Seism Soc Am 92(6):2323–2332

Ohta Y, Goto N (1978) Physical background of the statistically obtained S-wave velocity equation in terms of soil indexes. Butsuri-Tanko 31(1):8–17 (**in Japanese**)

Okada H (2003) The microseismic survey method: Society of Exploration Geophysicists of Japan. Geophysical Monograph Series No. 12. Society of Exploration Geophysicists.

Park CB, Miller RD, Xia J (1999) Multichannel analysis of surface waves. Geophysics 64(3):800–808

Pelekis PC, Athanasopoulos GA (2011) An overview of surface wave methods and a reliability study of a simplified inversion technique. Soil Dyn Earthq Eng 31(12):1654–1668

Piña-Flores J, Perton M, García-Jerez A, Carmona E, Luzón F, Molina-Villegas JC, Sánchez-Sesma FJ (2017) The inversion of spectral ratio H/V in a layered system using the diffuse field assumption (DFA). Geophys J Int 208(1):577–588

Poggi V, Fäh D (2010) Estimating Rayleigh wave particle motion from three-component array analysis of ambient vibrations. Geophys J Int 180(1):251–267

Sambridge M (1999) Geophysical inversion with a neighborhood algorithm—I. Searching a parameter space. Geophys J Int 138(2):479–494

Sánchez-Sesma FJ, Rodríguez M, Iturrarán-Viveros U, Luzon F, Campillo M, Margerin L, García-Jerez A, Suarez M, Santoyo MA, Rodríguez-Castellanos A (2011) A theory for microtremor H/V spectral ratio: application for a layered medium. Geophys J Int 186(1):221–225

Senna S, Wakai A, Suzuki H, Yatagai A, Matsuyama H, Fujiwara H (2018) Modeling of the subsurface structure from the seismic bedrock to the ground surface for a broadband strong motion evaluation in Kumamoto Plain. J Disaster Res 13(5):917–927

Socco LV, Boiero D (2008) Improved Monte Carlo inversion of surface wave data. Geophys Prospect 56:357–371

Tada T, Cho I, Shinozaki Y (2007) Beyond the SPAC method: exploiting the wealth of circular-array methods for microtremor exploration. Bull Seism Soc Am 97(6):2080–2095

Tada T, Cho I, Shinozaki Y (2010) New horizons in the utility of horizontal-motion microtremors, Proc. 7th International Conference on Urban Earthquake Engineering, Center for Urban Earthquake Engineering, Tokyo Institute of Technology.

Tokimatsu K, Tamura S, Kojima H (1992) Effects of multiple modes on Rayleigh wave dispersion characteristics. J Geotech Eng 118(10):1529–1543

Tsuno S, Nagashima F, Kawase H, Yamanaka H, Matsushima S (2023) Predicted results of the weak and strong ground motions at the target site of the blind prediction exercise as Step 2 and Step-3, -Report of the experiments for "The 6th International Symposium on Effects of Surface Geology on Seismic Motion", Earth, Planets and Space, submitted to this special volume.

Wathelet M, Jongmans D, Ohrnberger M (2004) Surface-wave inversion using a direct search algorithm and its application to ambient vibration measurements. Near Surf Geophys 2(4):211–221

Wathelet M, Jongmans D, Ohrnberger M (2005) Direct inversion of spatial auto correlation curves with the neighborhood algorithm. Bull Seism Soc Am 95(5):1787–1800

Wathelet M, Jongmans D, Ohrnberger M, Bonnefoy-Claudet S (2008) Array performances for ambient vibrations on a shallow structure and consequences over Vs inversion. J Seism 12:1–19

Wathelet M, Guillier B, Roux P, Cornou C, Ohrnberger M (2018) Rayleigh wave three-component beamforming: signed ellipticity assessment from high-resolution frequency-wavenumber processing of ambient vibration arrays. Geophys J Int 215(1):507–523

Wathelet M, Chatelain JL, Cornou C, Di Giulio G, Guillier B, Ohrnberger M, Savvaidis A (2020) Geopsy: a user-friendly open-source tool set for ambient vibration processing. Seism Res Lett 91(3):1878–1889

Yamanaka H (2007) Inversion of surface-wave phase velocity using hybrid heuristic search method. Butsuri-Tansa 60(3):265–275 (**in Japanese**)

Yamanaka H, Ishida H (1996) Application of genetic algorithms to an inversion of surface-wave dispersion data. Bull Seism Soc Am 86(2):436–444

Publisher's Note